Electronic Supplementary Material (ESI) for Nanoscale.

Supporting information for: From Electroburning to Sublimation: Substrate and Environmental Effects in the Electrical Breakdown Process of Monolayer Graphene

Maria El Abbassi,[*,†,§] László Pósa,[‡,§] Péter Makk,[†] Cornelia Nef,[†] Kishan Thodkar,[†] András Halbritter,[‡] and Michel Calame[†,¶,‖]

†*Department of Physics, University of Basel, Klingelbergstrasse 82, CH-4056 Basel, Switzerland*

‡*Department of Physics, Budapest University of Technology and Economics and MTA-BME Condensed Matter Research Group, 1111 Budapest, Budafoki ut 8, Hungary*

¶*Swiss Nanoscience Institute, University of Basel, 4056 Basel, Switzerland.*

§*Contributed equally to this work*

‖*Empa, Swiss Federal Laboratories for Materials Science and Technology, Transport at nanoscale interfaces Laboratory, CH-8600 Dubendorf, Switzerland.*

E-mail: maria.elabbassi@unibas.ch

Characterization of the junctions after EB

Estimation of the gap size by Simmons fitting

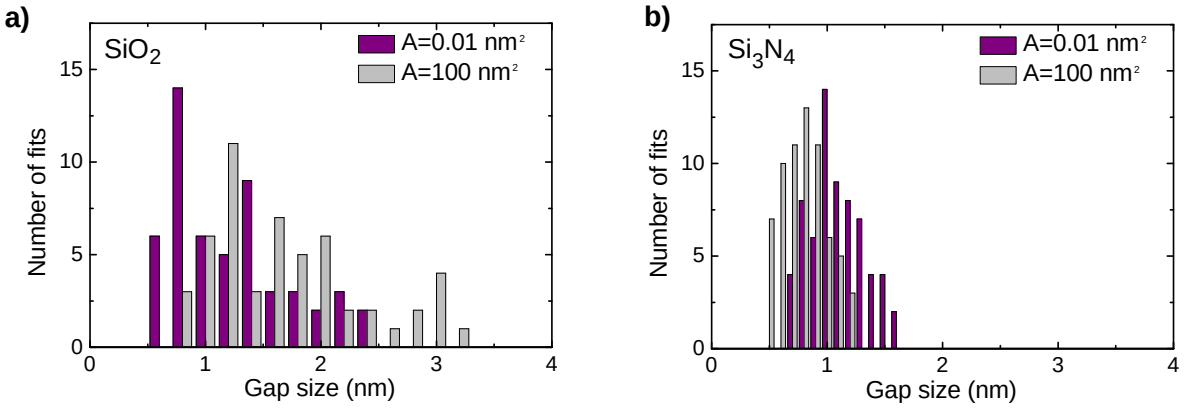

Figure S1: Histogram of the gap size estimation using a Simmons fitting after EB in vacuum. In purple, the fitting is performed by fixing the tunneling area to be 0.01 nm^2 and in grey to 100 nm^2. Panel a) corresponds to gaps on SiO_2 and b) to gaps on Si_3N_4.

When applying the Simmons fitting, one has to be careful, as fundamentally different junction area - gap width value combinations may provide very similar fitting curves. However, in case of graphene this problem is somewhat resolved, as we can anticipate that the junction area is larger than a single atom and smaller than the initial cross section of the graphene nanoribbon (400 nm width with single atom height). As we are uncertain about the actual junction area, we perform the Simmons fitting with these two limiting cross sections, and argue that the actual junction width is between the such obtained limiting values. This uncertainty in the junction area is accompanied by a sub-nm uncertainty in the gap size. More details about the fitting procedure are given in the supplementary information of our previous work [1]. After EB in vacuum, independently from the substrate, we get a narrow distribution of gap sizes around 1.5 nm (Fig.S1).

Gate dependence after EB

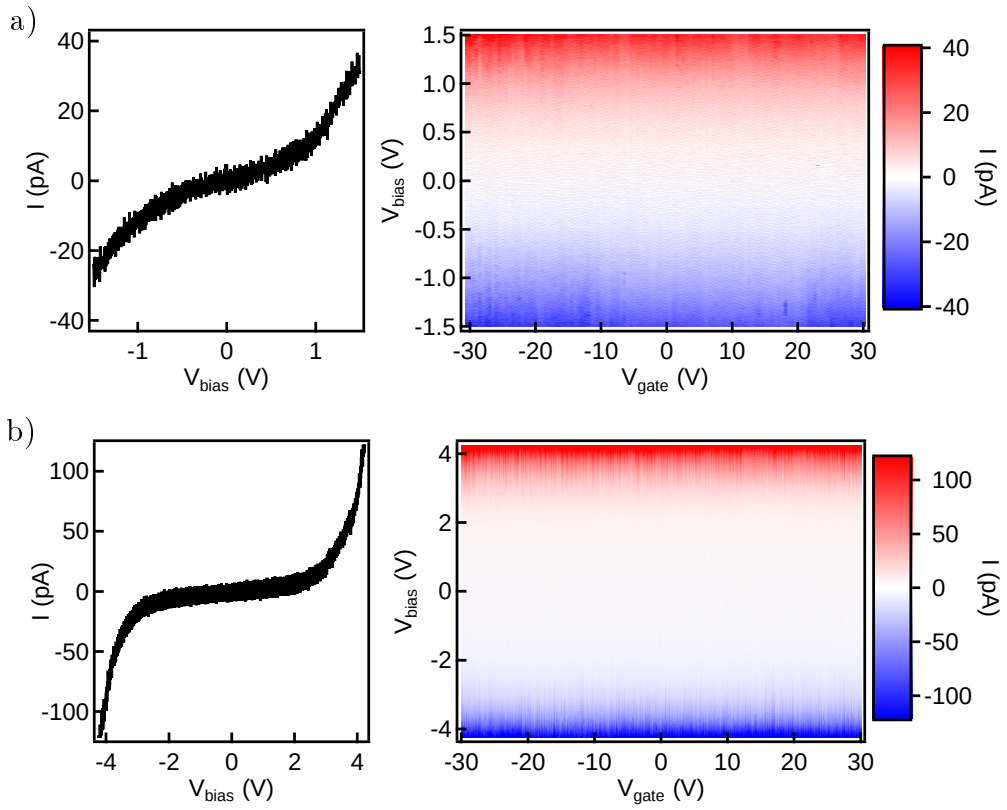

Figure S2: Characterization of one junction after EB: a) At room temperature; b) at 4K. The left panel corresponds to a typical I-V at zero gate voltage. The right panel corresponds to the gate dependent characterization of the gap. In both cases, no gate dependence is observed.

After EB systematic gate dependent measurements were performed at room temperature. For the majority of the devices (more than 70% of all devices) no gate dependence was observed, indicating the formation of empty gaps (see Fig.S2.a). As a further test two samples were also cooled down to 4.2K temperature justifying the absence of gate dependence (see Fig.S2.b). However, a minority of the samples exhibited gate dependent behavior (see Fig.S3), which we interpret by the presence of carbon islands in the gap. These devices all had relatively small zero bias resistance ($< 1G\Omega$).

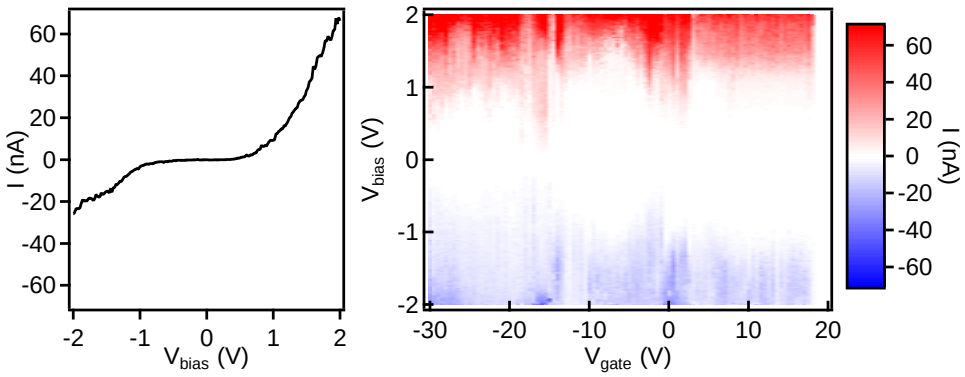

Figure S3: Room temperature characterization of a low resistance junction after EB. The left panel corresponds to a typical I-V at zero gate voltage. The right panel corresponds to the gate dependent characterization of the gap. Strong gate dependence is observed at room temperature.

Conversion from pulse length to number of oxygen molecules per atomic site

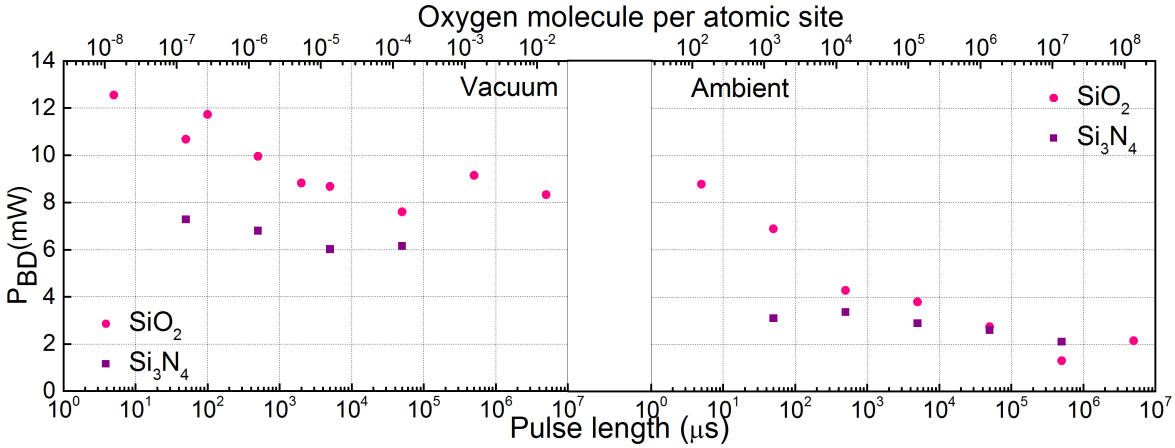

Figure S4: Average breakdown power of the graphene nanostructures on SiO_2 and on Si_3N_4 as a function of pulse length in vacuum and at ambient conditions. The common top axis is rescaled to the number of oxygen molecules arriving to a single atomic site during a single pulse.

In Fig. S4 the data of Fig. 2a of the manuscript are replotted using a common vertical top axis, which shows the average number of oxygen molecules arriving to a single atomic site during a single pulse.

Effect of the thermal transport parameters on the estimated junction temperature and the activation energies

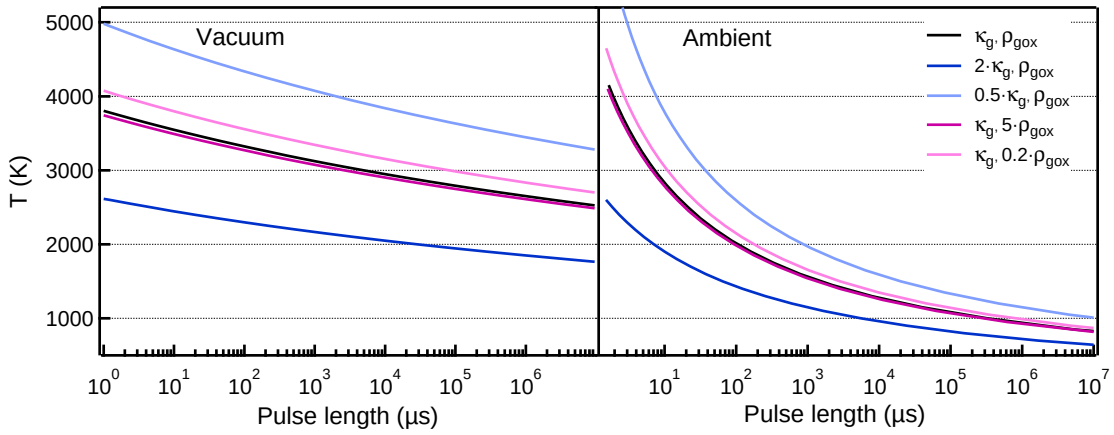

Figure S5: Effect of the thermal conductivity of graphene (κ_g) and the thermal boundary resistivity towards the SiO_2 substrate (ρ_{gox}) on the estimated breakdown temperature. The black curves are equivalent to the black fitting lines in Fig. 3 of the manusrcipt. First these curves are scaled back to breakdown power applying equation (1) of the main text with the thermal transport parameters used in the main text, and then these pulse length dependent power values are scaled to breakdown temperature using the same equation with detuned thermal tranport parameters.

As the estimation of the junction temperature relies on somewhat uncertain thermal transport parameters, we investigate the stability of our results against the variation of these factors in the case of the SiO_2 substrate. The heat conductivity of SiO_2 (κ_{ox}) is relatively well known (see main text), so we focus our analysis on the variation of the heat conductivity of graphene (κ_g) and the thermal boundary resistivity towards the SiO_2 substrate (ρ_{gox}). The black curves in Fig. S4 are replotting the black lines of Fig. 3 in the manuscript for ambient and vacuum conditions using a linear temperature scale instead of the Arrhenius plot. These curves are calculated using the reference thermal transport parameters, that were applied for our analysis in the main text. The blue/light blue curves demonstrate the calculated junction temperature using a doubled/halved thermal conductivity of graphene compared to the value used in the main text, and keeping the the thermal boundary resistivity towards the

substrate unchanged. The purple/pink curves demonstrate the estimated temperature using five times larger/smaller ρ_{gox} with unchanged κ_g. It is clear that the thermal conductivity of graphene has more pronounced influence on the junction temperature than the thermal boundary resistivity towards the substrate.

We have also calculated the activation energies corresponding to these detuned parameters, as shown by the table bellow. The results demonstrate that a factor of two detuning of κ_g yields only $\approx 20-30\%$ variation of the calculated activation energies, whereas a factor of five detuning of ρ_{gox} has even less influence on the results. Based on this analysis we can state that our results are stable against the chosen thermal transport parameters: in a broad interval of the these the estimated sublimation and burning activation energies remain consistent with the values known from the literature. The 7-8 times difference between the estimated activation energies in vacuum and in air is even less sensitive to the chosen parameters, clearly demonstrating the fundamental difference between the two breakdown processes.

	κ_g, ρ_{gox}	$2\kappa_g, \rho_{gox}$	$0.5\kappa_g, \rho_{gox}$	$\kappa_g, 5\rho_{gox}$	$\kappa_g, 0.2\rho_{gox}$
κ_g $(WK^{-1}m^{-1})$	1000	2000	500	1000	1000
ρ_{gox} (1E-8m^2 K/W)	1	1	1	5	0.2
E_a(eV) ambient	1.38	1.15	1.63	1.44	1.37
E_a(eV) vacuum	10.4	7.52	13.3	11.1	10.3

References

[1] C. Nef et al., Nanoscale, 2014, 6, 7249